

Label-free detection of polysulfides and glycogen of *Cyanidium caldarium* using ultra-multiplex coherent anti-Stokes Raman scattering microspectroscopy

Yuki Oka¹  | Masaki Yoshida² | Ayumi Minoda³ | Philippe Leproux⁴  | Makoto M. Watanabe²  | Hideaki Kano^{1,5} 

¹Department of Applied Physics, Graduate School of Pure and Applied Sciences, University of Tsukuba, Tsukuba, Japan

²Algae Biomass and Energy System R&D Center, University of Tsukuba, Tsukuba, Japan

³Faculty of Life and Environmental Sciences, University of Tsukuba, Tsukuba, Japan

⁴Institut de Recherche XLIM, Limoges, France

⁵Department of Chemistry, Faculty of Science, Kyushu University, Fukuoka, Japan

Correspondence

Hideaki Kano, Department of Chemistry, Kyushu University, 744, Motooka, Nishiku, Fukuoka-shi, Fukuoka 819-0395, Japan.
Email: hkano@chem.kyushu-univ.jp

Funding information

Japan Society for the Promotion of Science, Grant/Award Number: 18H02000

Abstract

Living microalga *Cyanidium caldarium* was visualized using ultra-multiplex coherent anti-Stokes Raman scattering (CARS) microspectroscopy. The Raman band related to the SO_4^{2-} ion at 982 cm^{-1} was detected at the peripheral part of the cells and showed a signal amplitude that was approximately threefold larger than that in the medium, indicating accumulation of SO_4^{2-} ions. Depending on the incubation conditions, a broad and sharp Raman band at approximately 505 cm^{-1} was observed at the peripheral part and inside the cells, respectively. Based on comparison of the results with model substances, these broad and sharp bands were assigned to polysulfides and glycogen, respectively.

KEYWORDS

algae, CARS, microscopy, microspectroscopy, supercontinuum

1 | INTRODUCTION

Recently, Raman spectroscopy has attracted much attention as a single-cell analytical method for investigating microalgae without cell disruption. Thanks to the molecular specific vibrational contrast, various kinds of intracellular metabolites can be visualized in a label-free manner. Moudříková et al.^[1] applied confocal spontaneous Raman microscopy to the microalga *Chlorella vulgaris* and revealed the intracellular distribution of polyphosphoric acid. Samek et al.^[2] determined the effective iodine value in lipid storage bodies of the individual living microalgae *Chlamydomonas* sp. and

Botryococcus sudeticus by spontaneous Raman microscopy. Heraud et al.^[3] performed spontaneous Raman microscopy of *Dunaliella tertiolecta* and predicted the nutrient status of individual algal cells.

Moreover, coherent Raman scattering microscopies, such as coherent anti-Stokes Raman scattering (CARS) microscopy and stimulated Raman scattering (SRS) microscopy, have also been applied to investigate intracellular metabolites. In coherent Raman scattering, two laser pulses with different colors are used: ω_1 (pump) and ω_2 (Stokes) pulses. If the wavenumber difference ($\omega_1 - \omega_2$) of the two incident laser pulses coincides with the specific wavenumber (Ω) of the vibrational mode of

the sample molecule, namely, $\omega_1 - \omega_2 = \Omega$, the vibrational mode of a large number of sample molecules is resonantly and coherently excited. The vibrational coherence generated in this process is converted to ω_{CARS} or ω_{SRS} radiation through the interaction of molecules with the third laser pulses (ω_1 for CARS and ω_2 for SRS [stimulated Raman loss]). Cavanaugh et al.^[4] applied CARS microscopy to the microalga *Phaeodactylum tricornutum* and found that the organism uses two different modes for normal and excessive lipid accumulation processes. Hiramatsu et al.^[5] applied a Fourier transform CARS flow cytometer to evaluate the microalga *Haematococcus lacustris* and measured the synthesis of astaxanthin molecules. He et al.^[6] applied CARS microscopy to the microalga *Coccomyxa subellipsoidea* C169 and reported that the Raman signal of lipid droplets appeared after N-depletion. Wakisaka et al.^[7] performed label-free video-rate metabolite imaging of the microalga *Euglena gracilis* by SRS microscopy and observed the intracellular metabolite distributions under different culture conditions. Wang et al.^[8] applied frequency-modulated SRS microscopy to *Botryococcus braunii* and visualized intracellular lipid droplets and extracellular hydrocarbons. Particularly, ultra-multiplex CARS spectroscopic imaging was shown to be a powerful method for identifying molecular species in a label-free manner under a microscope.^[9–12] We performed ultra-multiplex CARS microspectroscopic imaging^[12–14] of *Aurantiochytrium mangrovei*, revealing intracellular accumulation of squalene in vacuoles.^[15] In the present study, we applied this technique to the living alga *Cyanidium caldarium* to detect hitherto unknown metabolites.

C. caldarium is a historically well-studied strain in Cyanidiophyceae, which can survive at low pH values from 0.5 to 4.0 and temperatures from 35 to 56°C in their natural environments, including acid hot springs and moist acid soils.^[16,17] *C. caldarium* is a red alga but lacks the red pigment phycoerythrin. Therefore, the cells exhibit a blue-green color. It is known as a good model system to understand the traits of photosynthetic eukaryotes and extremophiles.^[17–19] Further, its biological application for biofuel production, urban wastewater treatment, and precious metal recycling has been receiving attention in recent years.^[20–23]

Cyanidiophyceae comprises *Cyanidium*, *Cyanidioschyzon*, and *Galdieria*. Of the three species, only *Cyanidioschyzon* has no obvious cell wall, whereas *Cyanidium* and *Galdieria* contain a layered rigid cell wall.^[24,25] The rigid cell wall gives these species a higher tolerance to environmental stresses, including high salinity and high osmolarity, compared with *Cyanidioschyzon*.^[17] However, it makes morphological

and biochemical analyses in these species difficult. Thus, label-free single-cell analysis of *C. caldarium* will overcome the problem and provide new insights into the biology of Cyanidiophyceae.

2 | EXPERIMENTAL

2.1 | Setup

Figure 1 shows the experimental setup of the homebuilt multimodal nonlinear optical microscopic system.^[14] This system enables acquisition of ultra-multiplex CARS, second harmonic generation (SHG), and third harmonic generation (THG) signals. The main laser source was a custom-made, dual-fiber output synchronized laser source (OPERA HP, Leukos, Limoges, France). In the laser housing, the master laser output, with a wavelength of 1064 nm, temporal duration of 50 ps, and repetition rate of 1 MHz, was divided into two. One was introduced into the large-mode area photonic crystal fiber (PCF) and used as the pump beam, ω_1 , which was collimated by a collimator lens (F810APC-1064, Thorlabs, Newton, NJ, USA). The other was injected into the PCF with high nonlinearity to obtain ultra-broadband supercontinuum (SC) radiation ranging from visible to near infrared (NIR). The NIR spectral components of the SC were selected using an optical filter (IR80, Kenko-optics, Tokyo, Japan) and were used as the Stokes beam (ω_2). The SC was collimated by an off-axis parabolic mirror (RC04APC-P01, Thorlabs) to avoid chromatic dispersion. The two beams were superimposed by a notch filter (NF03-532/1064E-25, Semrock, Rochester, NY, USA) and guided into a modified inverted microscope (ECLIPSE Ti with modification, Nikon, Tokyo, Japan) in collinear geometry. Two laser beams were tightly focused on the sample through a microscope objective (CFI Plan Apo 60× NA 1.27, water immersion, Nikon). The sample was placed on a piezoelectric stage (Nano-LP200, Mad City Labs, Madison, WI, USA) for three-dimensional (xyz) position selection. The full scanning range of the xyz-piezo stage was 200 μm^3 . The sample on the piezo stage was raster-scanned (first in the horizontal direction and then in the vertical direction). The SHG, THG, and ultra-multiplex CARS signals were collected using a second objective lens (Plan S Fluor 40× NA 0.6, Nikon) and spectrally separated by a dichroic mirror. The CARS signal transmitted through the dichroic mirror was detected using a spectrometer (LS785, Princeton Instruments, Trenton, NJ, USA) equipped with a charge-coupled device (CCD) camera (BLAZE 100HR, Princeton Instruments). The spectral coverage and spectral resolution of the CARS signal were ~ 3500 and 8 cm^{-1} , respectively. The SHG and

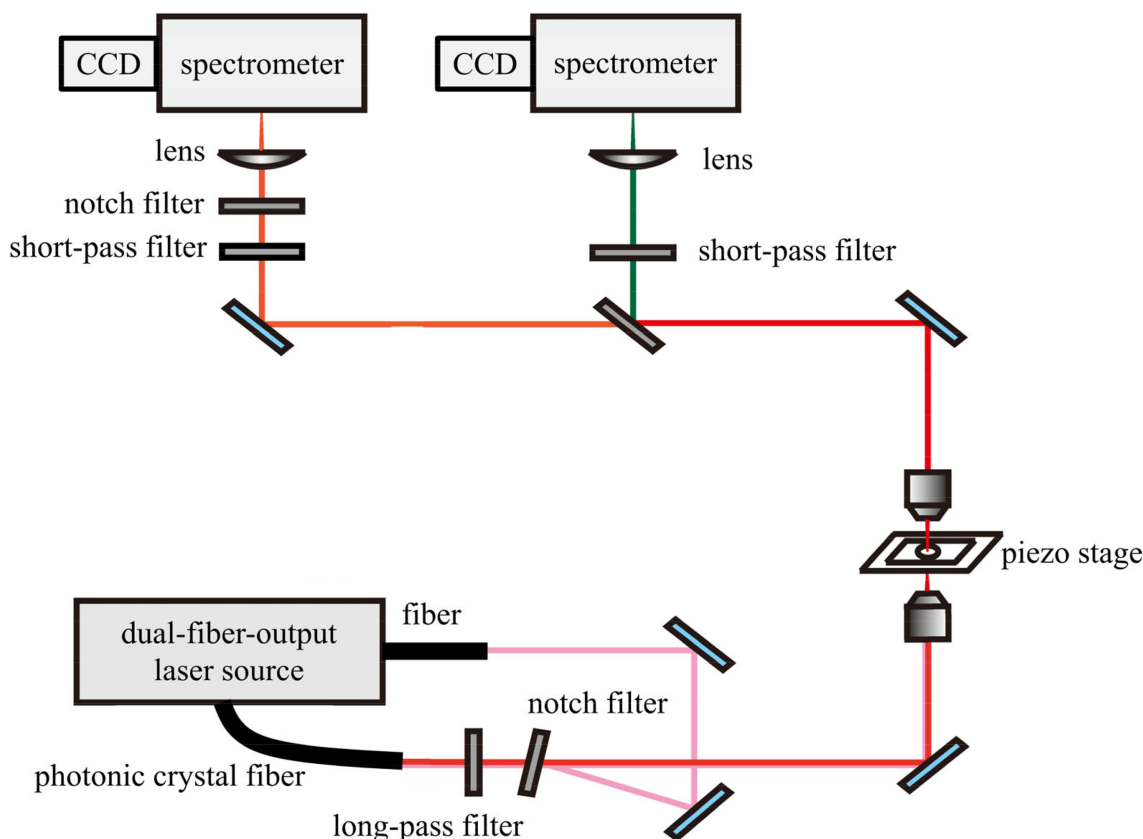


FIGURE 1 Experimental setup of ultra-multiplex spectroscopic CARS system with SHG and THG channels

THG signals reflected by the dichroic mirror were detected using a spectrometer (SpectraPro300i, Princeton Instruments) equipped with a CCD camera (PIXIS 100B, Princeton Instruments). The exposure time at each spatial position was 50 ms for signal detection. The image size (pixels and microns) and step size were 101×101 pixels, $50 \times 50 \mu\text{m}^2$, and $0.5 \mu\text{m}$, respectively.

2.2 | Sample preparation

C. caldarium NIES-2137 was obtained from the NIES culture collection (National Institute for Environmental Studies, Onogawa, Japan). The strain was maintained in glass test tubes containing 10 mL of M-Allen medium,^[26] with the pH adjusted to 2.0 with H_2SO_4 . The temperature of the incubator (BioTRON LH-240SP, NK System, Tokyo, Japan) was set to 35°C with continuous white fluorescent light (Panasonic, Osaka, Japan, $80 \mu\text{mol m}^{-2} \text{s}^{-1}$) without agitation. Before the measurements, the strain in the glass tube was maintained for 16 and 47 days at room temperature (20.9°C) after the last incubation and was used as the sample. For microscopy, a $5 \mu\text{L}$ drop of M-Allen medium containing living cells

was sandwiched on a slide glass and cover slip, which were sealed with nail polish.

Na_2S_4 (Dojindo Molecular Technologies, Rockville, MD, USA) and glycogen (FUJIFILM Wako, Osaka, Japan) were used without further purification.

3 | RESULTS AND DISCUSSION

Figure 2a shows an optical image of living *C. caldarium* cells, which ranged in size from 2 to $10 \mu\text{m}$ in diameter. The green pigments correspond to chloroplasts. Figure 2b shows a CARS intensity mapping of the same area shown in Figure 2a, which was mapped using the CARS signal intensity at 1653 cm^{-1} (vertical dashed line in Figure 2c), corresponding to the apparent peak of the dispersion lineshape. The laser power was approximately 170 and 80 mW for the pump and Stokes, respectively. The band around 1653 cm^{-1} corresponds to amide I and/or *cis* $\text{C}=\text{C}$ stretching vibrational modes. Therefore, the CARS intensity mapping in Figure 2b corresponds to the superposition of the images due to proteins and lipids. It should be noted that the cell debris floating in the medium, which is not observed in the optical image,

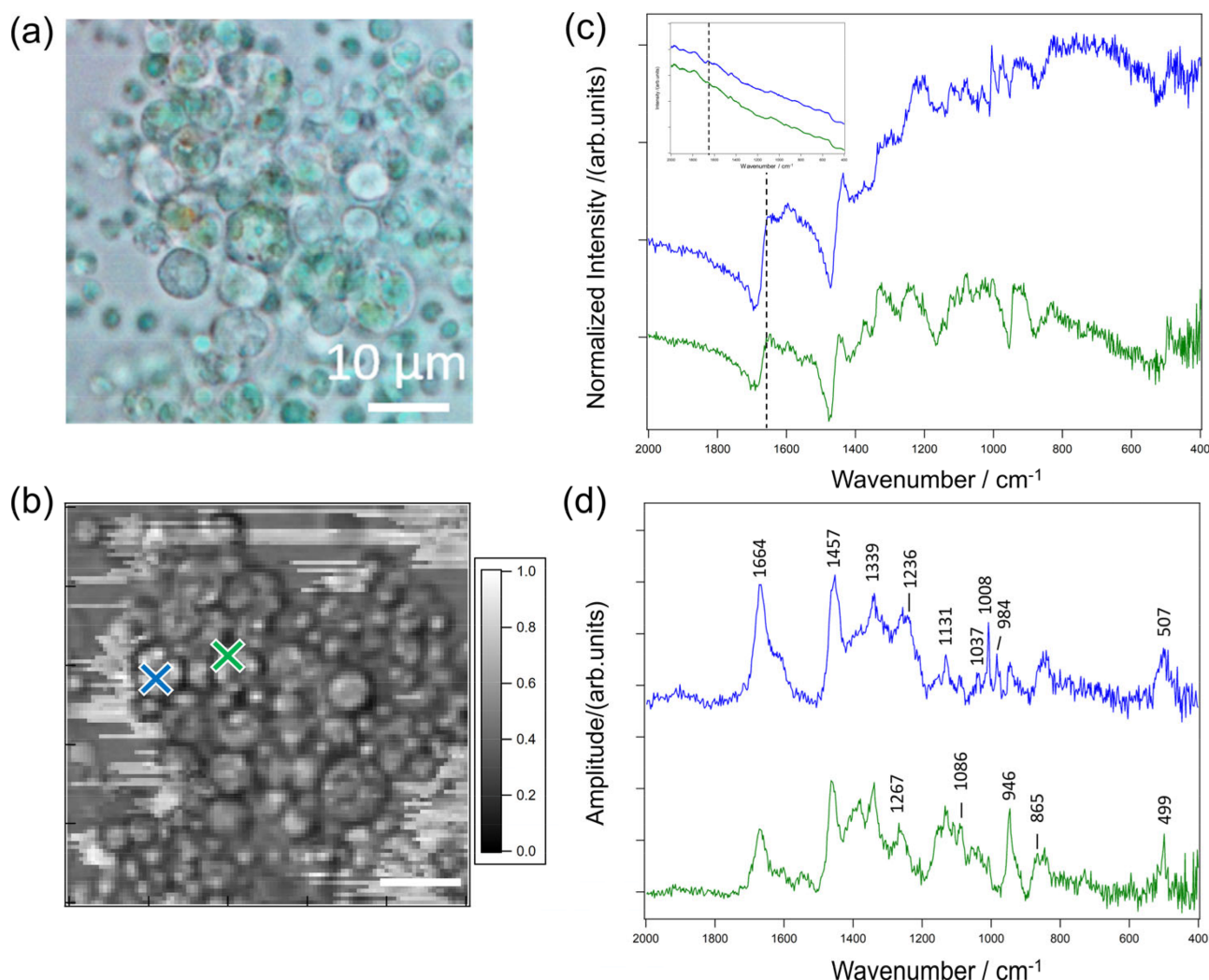


FIGURE 2 (a) Optical image of *Cyanidium caldarium*. (b) CARS intensity mapping at 1653 cm^{-1} . (c) Spectral profile of the raw CARS signal at the position indicated in (b). (d) $\text{Im}[\chi^{(3)}]$ spectra calculated from (c). The sample was maintained for 47 days at room temperature (20.9°C) after nutrients in the medium were exchanged

gives an artificial image contrast in Figure 2b, especially at the upper and lower right areas of the images. The cell debris in the medium was tweezed by the laser beam and was moved to the horizontal direction in the image during the raster scanning of the sample. The inset of Figure 2c shows the raw CARS spectra at two different intracellular positions (blue and green crosses) in Figure 2b. Because the raw CARS signals are distorted mainly by the spectral profile of the Stokes pulses and diffraction efficiency of the spectrometer, we performed spectral correction of this signal by dividing the raw CARS spectra by the spectral profile of the medium, which is considered as non-resonant background (NRB). The resulting intensity-corrected CARS spectra are shown in Figure 2c. The spectral profiles are dispersive because the vibrationally resonant signal and NRB interfere with each other. We next retrieved the pure

vibrationally resonant spectra, which corresponded to the imaginary part of the $\chi^{(3)}$ ($\text{Im}[\chi^{(3)}]$) spectra, from the spectra shown in Figure 2c using the maximum entropy method.^[27] The $\text{Im}[\chi^{(3)}]$ spectra with background subtraction are shown in Figure 2d.

As indicated in Figure 2d, the $\text{Im}[\chi^{(3)}]$ spectra showed characteristic Raman bands at 1664, 1457, 1339, 1267, 1236, 1131, 1086, 1037, 1008, and 982 cm^{-1} , corresponding to amide I and/or *cis* C=C stretching, CH_3 degenerate deformation, CH deformation, =C-H bending, amide III, skeletal C-C (*trans*) stretching, skeletal C-C (*gauche*) stretching, in-plane phenyl ring deformation, phenyl ring breathing, and SO_4^{2-} symmetric stretching vibrational modes, respectively.^[10,12]

By analyzing the spectral profile at each cell position, we reconstructed the CARS images at various Raman bands. Figure 3 summarizes the results of ultra-multiplex

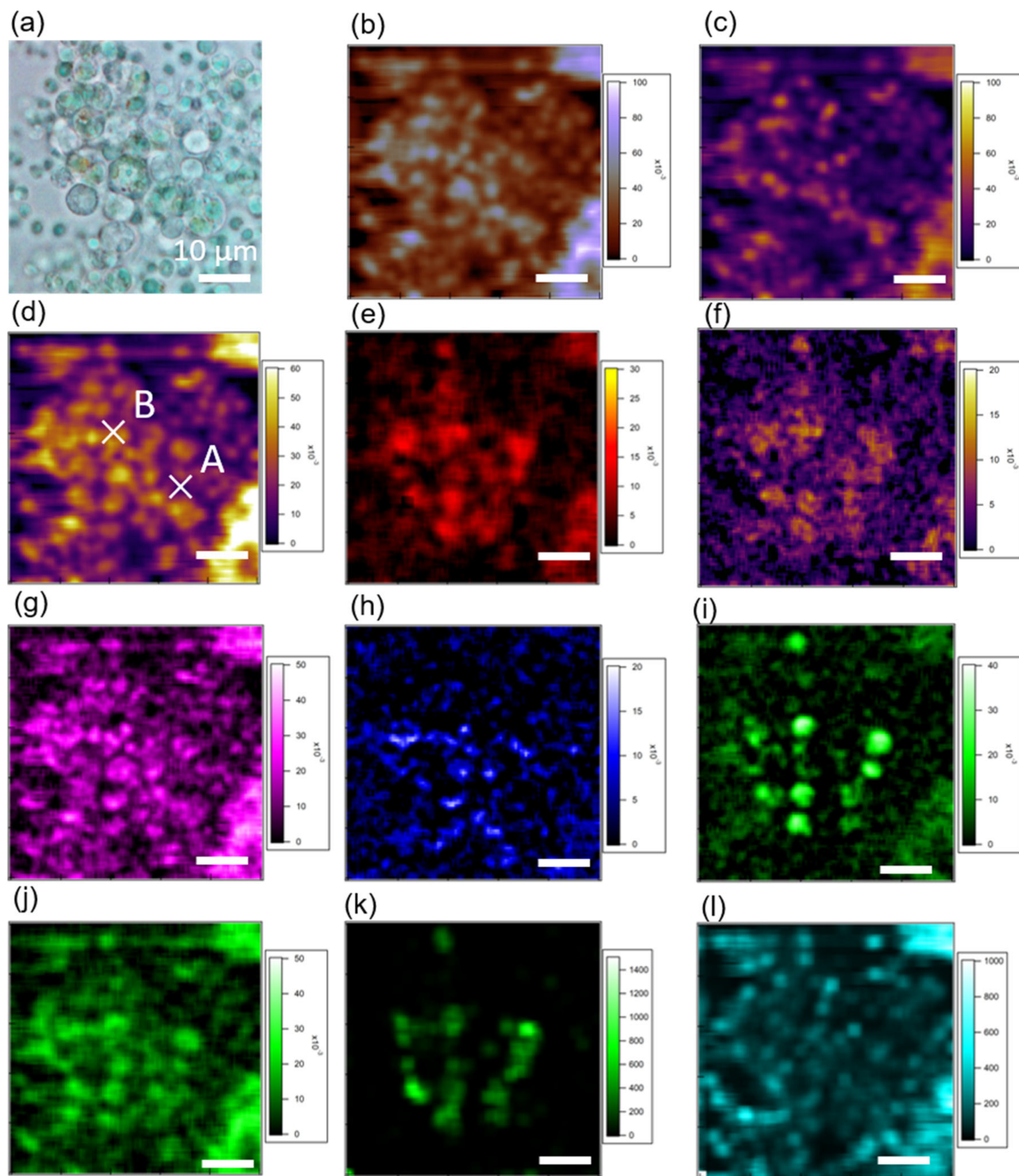


FIGURE 3 (a) Optical image (same image as in Figure 2a); CARS images of *C. caldarium* around (b) 1664, (c) 1610, (d) 1457, (e) 1267, (f) 1037, (g) 1008, (h) 982, (i) 944, and (j) 860 cm^{-1} , (k) SHG, (l) THG. These images are averaged over $2 \mu\text{m}^2$ (see the text). The sample was maintained for 47 days at room temperature (20.9°C) after nutrients in the medium were exchanged

CARS imaging. Because the signal-to-noise ratio was not high in the fingerprint region, the Raman band at each position was first averaged over $2 \mu\text{m}^2$ and then fitted by the Gaussian function. The fitted results around 1660 and

1000 cm^{-1} , where several Raman bands are congested in the fingerprint region, are shown in Figure S1. Finally, the fitted result was mapped out. The CARS images without spatial averaging are also indicated in Figure S2.

Figure 3b–j shows the CARS images around 1664 (b), 1610 (c), 1457 (d), 1267 (e), 1037 (f), 1008 (g), 982 (h), 944 (i), and 860 (j) cm^{-1} . The CARS images in Figure 3 were classified into two main categories. First, those exhibiting image contrast similar to that of the optical image are shown in Figures 3b,d,g. Second, specific cells with high image contrast are shown in Figure 3c,e,f,h,i,j. Among them, the CARS image at 982 cm^{-1} (Figure 3h) showed high image contrast at the peripheral parts of the cells. The CARS signal amplitude at 982 cm^{-1} at the peripheral parts of the cells was approximately threefold larger than that outside of the cells (Figure S3). As the band at 982 cm^{-1} was assigned to the SO_4^{2-} ion, the image reveals the accumulation of SO_4^{2-} ions at the peripheral parts of the cells.

Figure 3k,l shows the SHG and THG images. As discussed later, the SHG image is similar to the CARS images at the Raman shifts of 944 (Figure 3i) and 860 cm^{-1} (Figure 3j). On the other hand, the THG image is similar to the CARS images at the Raman shifts of 1664 (Figure 3b) and 1457 cm^{-1} (Figure 3d) visualizing intracellular lipids.^[10]

During spectroscopic analysis, we found that two Raman bands with different bandwidths overlapped at

approximately 505 cm^{-1} . Figure 4a shows the spectral profiles at two intracellular positions, A and B. The $\text{Im}[\chi^{(3)}]$ spectrum at Position A (red) showed a broad spectral profile. In contrast, the broad and sharp bands were superposed at Position B (green). To decompose the two spectral components with broad and sharp bandwidths, we fitted the spectral profile around 505 cm^{-1} by determining the sum of the broad and sharp Gaussian functions, whose full width at half maxima were about 60 and 19 cm^{-1} , respectively. The broad and sharp Gaussian functions are indicated in Figure 4a,d, whereas Figure 4b,c shows the decomposed CARS image of the broad and sharp spectral components, respectively. The CARS image of the broad band clearly gives a high image contrast at the peripheral parts of the cells.

We next considered the molecular origin of the broad band. A Raman band around 505 cm^{-1} is typically observed in biomolecules containing disulfide bonds (S–S). According to a previous study,^[25] the acid- and heat-resistant *C. caldarium* has cell walls that are unusually rich in protein (50%–55%). Therefore, one candidate is proteins containing amino acids, such as cysteine (Cys), which can form interchain disulfide bonds (Cys–Cys). However, the observed spectral profile (A in

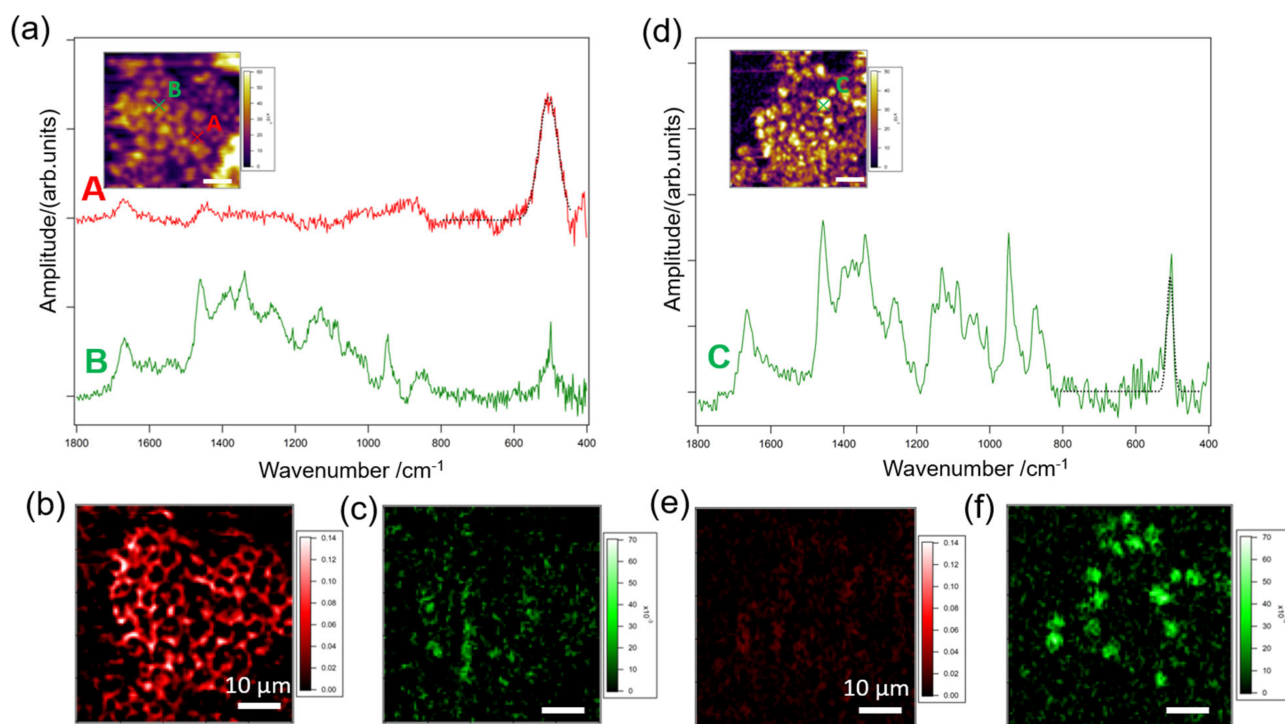


FIGURE 4 (a) Spatially averaged $\text{Im}[\chi^{(3)}]$ spectra (solids) at Areas A and B and the fitted result (dotted). The sum of the broad and sharp Gaussian functions was used to fit the spectral profile around 505 cm^{-1} . CARS images of the (b) broad (FWHM: 60 cm^{-1}) and (c) sharp (FWHM: 19 cm^{-1}) Raman bands. These images are averaged over $2 \mu\text{m}^2$. (d) Spatially averaged $\text{Im}[\chi^{(3)}]$ spectrum (solid) at Area C and the fitted result (dotted). CARS images of the (e) broad and (f) sharp Raman bands. These images are averaged over $2 \mu\text{m}^2$. The results shown in (a–c) and (d–f) were obtained using live algae, which were maintained for 47 and 16 days at room temperature (20.9°C) after nutrients in the medium were exchanged

Figure 4a) shows a prominent band only around 505 cm^{-1} without the typical band generated by proteins.^[28,29] Therefore, the band around 505 cm^{-1} could not be assigned to a disulfide bond in Cys-Cys.

Another candidate is polysulfides. A previous study showed that the red alga *Chondria californica* produces cyclic polysulfides.^[30] Many studies have focused on the Raman band due to polysulfides from the perspective of battery fabrication. Solid-phase polysulfides showed a Raman band similar to that observed. Janz et al.^[31] reported a band at 488 cm^{-1} for Na_2S_5 . Steudel and Chivers^[32] reported bands at 505, 494, 450, 424, and 410 cm^{-1} for solid-state Cs_2S_6 . All of these bands were assigned as S-S stretching vibrational modes. Chivers et al.^[33] reported bands at 503, 453, 419, and 395 cm^{-1} for S_7^{2-} ion in $[\text{PPN}]_2\text{S}_7 \cdot 2\text{EtOH}$, all of which were also assigned as S-S stretching vibrational modes. Nims et al.^[34] reported a band at 473 cm^{-1} , with a shoulder feature at $\sim 467\text{ cm}^{-1}$, for solid S_8 allotropes, which were assigned as S-S bond stretching of the S_8 ring structure. Wu et al.^[35] reported bands at 518 cm^{-1} for S_4^{2-} and 534 cm^{-1} for S_3 . Janz et al.^[31] reported bands at

458 and 476 cm^{-1} in BaS_3 , which were assigned to S-S stretching at 25°C . Khan et al.^[36] reported a band at 450 cm^{-1} for S_4^{2-} or S_5^{2-} and at 495 cm^{-1} for S_5^{2-} in a polysulfide solution with an S:Na ratio of 1.8 in 1.8 mol dm^{-3} aqueous Na_2S solution. Hagen et al.^[37] reported DFT calculations of S_7^{2-} and S_8^{2-} , which produce Raman bands at 486 and 487 cm^{-1} , respectively.

We then measured the polysulfides to compare the intracellular Raman band around 505 cm^{-1} with that of a model polysulfide-containing substance. Figure 5c shows the $\text{Im}[\chi^{(3)}]$ spectrum of Na_2S_4 , which was obtained with the same setup used to measure living cells. The main band in the spectrum was observed around 505 cm^{-1} , which coincides well with the Raman band observed in *C. caldarium*. Therefore, the broad Raman band around 505 cm^{-1} is likely assignable to S-S stretching vibrational modes of polysulfides.

A sharp Raman band was also observed around 505 cm^{-1} . Based on analysis of the spectroscopic images, the sharp band was accompanied by Raman bands at 865 and 946 cm^{-1} (Figure 5b). These Raman bands are known as markers of polysaccharides, such as glycogen

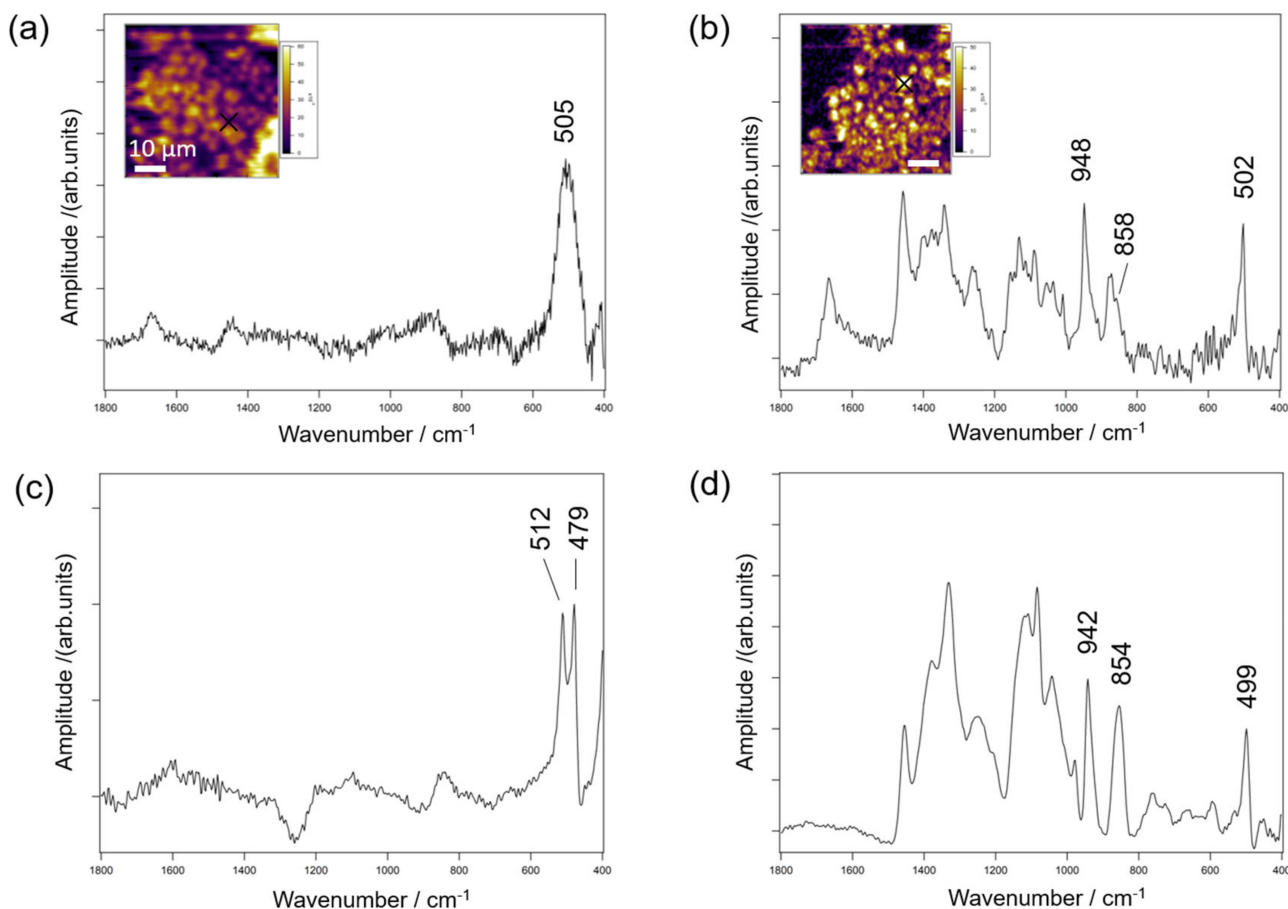


FIGURE 5 (a) $\text{Im}[\chi^{(3)}]$ spectrum at the intracellular positions indicated as A in Figure 4a. (b) $\text{Im}[\chi^{(3)}]$ spectrum at the positions indicated as C in Figure 4b. $\text{Im}[\chi^{(3)}]$ spectra of Na_2S_4 (c) and glycogen (d)

and starch. According to the literature, *C. caldarium* accumulates glycogen in the cytosol.^[38,39] This property is unique compared with green algae and terrestrial plants, which store starch in their chloroplasts. We compared the spectral profile showing a sharp band around 505 cm⁻¹ (Figure 5b) with a model substance of glycogen. As the main spectroscopic features were reproduced, we assigned the molecular species observed in *C. caldarium* to glycogen. Interestingly, the CARS images due to glycogen (Figure 3i,j) gave similar image contrast to the SHG image (Figure 3k), indicating that accumulated glycogen inside cells is SHG active.

4 | CONCLUSION


In conclusion, we successfully visualized intracellular polysulfides in living *C. caldarium* cells, which showed a spectroscopic signature around 505 cm⁻¹ with a broad bandwidth of 60 cm⁻¹. Depending on the incubation conditions, intracellular glycogen was also visualized as a sharp Raman band around 505 cm⁻¹ with a sharp bandwidth of 19 cm⁻¹. Based on our spectroscopic analysis, polysulfides and glycogen were spectrally separated to obtain each CARS image, demonstrating that polysulfides and glycogen were exclusively localized. Our approach provides a foundation for developing a new label-free rapid cell screening method to identify unknown metabolites.

ACKNOWLEDGEMENTS

The authors gratefully acknowledge the assistance of J. Ukon of Ukon Craft Science, Ltd., for establishing a fruitful collaboration between Japanese and French laboratories. This study was financially supported by Japan Society for the Promotion of Science KAKENHI Grant Number 18H02000 (Grant-in-Aid for Scientific Research [B]). This work benefited from French government support managed by the National Research Agency under the Investments for the Future program with the reference ANR-10-LABX-0074 Sigma-LIM.

ORCID

Yuki Oka  <https://orcid.org/0000-0002-2522-3505>

Philippe Leproux  <https://orcid.org/0000-0002-3854-413X>

Makoto M. Watanabe  <https://orcid.org/0000-0003-3267-7270>

Hideaki Kano  <https://orcid.org/0000-0003-3682-7627>

REFERENCES

- [1] Š. Moudříková, A. Sadowsky, S. Metzger, L. Nedbal, T. Mettler-Altmann, P. Mojžeš, *Anal. Chem.* **2017**, *89*, 12006.
- [2] O. Samek, A. Jonáš, Z. Pilát, P. Zemánek, L. Nedbal, J. Triska, P. Kotas, M. Trtílek, *Sensors* **2010**, *10*, 8635.
- [3] P. Heraud, J. Beardall, D. McNaughton, B. R. Wood, *FEMS Microbiol. Lett.* **2007**, *275*, 24.
- [4] L. Cavanaugh, H. Fink, J. Kiskis, E. Albers, I. Undeland, A. Enejder, *Plant Physiol.* **2015**, *167*, 603.
- [5] K. Hiramatsu, T. Ideguchi, Y. Yonamine, S. Lee, Y. Luo, K. Hashimoto, T. Ito, M. Hase, J.-W. Park, Y. Kasai, S. Sakuma, T. Hayakawa, F. Arai, Y. Hoshino, K. Goda, *Sci. Adv.* **2019**, *5*, eaau0241.
- [6] X. N. He, J. Allen, P. N. Black, T. Baldacchini, X. Huang, H. Huang, L. Jiang, Y. F. Lu, *Biomedical Optics Express* **2012**, *3*, 2896.
- [7] Y. Wakisaka, Y. Suzuki, O. Iwata, A. Nakashima, T. Ito, M. Hirose, R. Domon, M. Sugawara, N. Tsumura, H. Watarai, T. Shimobaba, K. Suzuki, K. Goda, Y. Ozeki, *Nature Microbiology* **2016**, *1*, 16124.
- [8] W. Chun-Chin, C. Dayananda, S. Nicholas, M. Julian In Proc. SPIE **2015**, 9329.
- [9] C. H. Camp Jr., M. T. Cicerone, *Nat. Photonics* **2015**, *9*, 295.
- [10] H. Yoneyama, K. Sudo, P. Leproux, V. Couderc, A. Inoko, H. Kano, *APL Photonics* **2018**, *3*, 092408.
- [11] F. Sinjab, K. Hashimoto, V. R. Badarla, J. Omachi, T. Ideguchi, *Opt. Express* **2020**, *28*, 20794.
- [12] H. Kano, T. Maruyama, J. Kano, Y. Oka, D. Kaneta, T. Guerenne, P. Leproux, V. Couderc, M. Noguchi, *OSA Continuum* **2019**, *2*, 1693.
- [13] H. Kano, H. Hamaguchi, *Appl. Phys. Lett.* **2005**, *86*, 121113.
- [14] D. Kaneta, M. Goto, M. Hagihara, P. Leproux, V. Couderc, M. Egawa, H. Kano, *Analyst* **2021**, *146*, 1163.
- [15] K. Ishitsuka, M. Koide, M. Yoshida, H. Segawa, P. Leproux, V. Couderc, M. M. Watanabe, H. Kano, *J. Raman Spectrosc.* **2017**, *48*, 8.
- [16] J. Seckbach, *Evolutionary Pathways and Enigmatic Algae: Cyanidium caldarium (Rhodophyta) and Related Cells*, Kluwer Academic Publishers, Dordrecht **1994**.
- [17] V. Reeb, D. Bhattacharya, *Red Algae in the Genomic Age*, Springer, Dordrecht **2010**.
- [18] M. Matsuzaki, O. Misumi, T. Shin-i, S. Maruyama, M. Takahara, S.-y. Miyagishima, T. Mori, K. Nishida, F. Yagisawa, K. Nishida, Y. Yoshida, Y. Nishimura, S. Nakao, T. Kobayashi, Y. Momoyama, T. Higashiyama, A. Minoda, M. Sano, H. Nomoto, K. Oishi, H. Hayashi, F. Ohta, S. Nishizaka, S. Haga, S. Miura, T. Morishita, Y. Kabeya, K. Terasawa, Y. Suzuki, Y. Ishii, S. Asakawa, H. Takano, N. Ohta, H. Kuroiwa, K. Tanaka, N. Shimizu, S. Sugano, N. Sato, H. Nozaki, N. Ogasawara, Y. Kohara, T. Kuroiwa, *Nature* **2004**, *428*, 653.
- [19] G. Schönknecht, W.-H. Chen, C. M. Ternes, G. G. Barbier, R. P. Shrestha, M. Stanke, A. Bräutigam, B. J. Baker, J. F. Banfield, R. M. Garavito, K. Carr, C. Wilkerson, S. A. Rensing, D. Gagneul, N. E. Dickenson, C. Oesterheld, M. J. Lercher, A. P. M. Weber, *Science* **2013**, *339*, 1207.
- [20] T. Sakurai, M. Aoki, X. Ju, T. Ueda, Y. Nakamura, S. Fujiwara, T. Umemura, M. Tsuzuki, A. Minoda, *Bioresour. Technol.* **2016**, *200*, 861.
- [21] X. Ju, K. Igarashi, S.-i. Miyashita, H. Mitsuhashi, K. Inagaki, S.-i. Fujii, H. Sawada, T. Kuwabara, A. Minoda, *Bioresour. Technol.* **2016**, *211*, 759.
- [22] T. Selvaratnam, A. K. Pegallapati, F. Montelya, G. Rodriguez, N. Nirmalakhandan, W. Van Voorhies, P. J. Lammers, *Bioresour. Technol.* **2014**, *156*, 395.

- [23] A. Minoda, H. Sawada, S. Suzuki, S.-i. Miyashita, K. Inagaki, T. Yamamoto, M. Tsuzuki, *Appl. Microbiol. Biotechnol.* **2015**, 99, 1513.
- [24] P. Albertano, C. Ciniglia, G. Pinto, A. Pollio, *Hydrobiologia* **2000**, 433, 137.
- [25] R. W. Bailey, L. A. Staehelin, *Microbiology* **1968**, 54, 269.
- [26] A. Minoda, R. Sakagami, F. Yagisawa, T. Kuroiwa, K. Tanaka, *Plant Cell Physiol.* **2004**, 45, 667.
- [27] E. M. Vartiainen, H. A. Rinia, M. Müller, M. Bonn, *Opt. Express* **2006**, 14, 3622.
- [28] A. Kuzuhara, *J. Mol. Struct.* **2014**, 1076, 373.
- [29] N. N. Brandt, A. Y. Chikishev, A. V. Golovin, V. N. Kruzhilin, A. O. Zalevsky, *Biomedical Spectroscopy and Imaging* **2014**, 3, 287.
- [30] S. J. Wratten, D. J. Faulkner, *J. Org. Chem.* **1976**, 41, 2465.
- [31] G. J. Janz, E. Roduner, J. W. Coutts, J. R. Downey, *Inorg. Chem.* **1976**, 15, 1751.
- [32] R. Steudel, T. Chivers, *Chem. Soc. Rev.* **2019**, 48, 3279.
- [33] T. Chivers, F. Edelmann, J. F. Richardson, K. J. Schmidt, *Can. J. Chem.* **1986**, 64, 1509.
- [34] C. Nims, B. Cron, M. Wetherington, J. Macalady, J. Cosmidis, *Sci. Rep.* **2019**, 9, 7971.
- [35] H.-L. Wu, L. A. Huff, A. A. Gewirth, *ACS Appl. Mater. Interfaces* **2015**, 7, 1709.
- [36] S. A. Khan, R. W. Hughes, P. A. Reynolds, *Vib. Spectrosc.* **2011**, 56, 241.
- [37] M. Hagen, P. Schiffels, M. Hammer, S. Dörfler, J. Tübke, M. J. Hoffmann, H. Althues, S. Kaskel, *J. Electrochem. Soc.* **2013**, 160, A1205.
- [38] S. O. Konorov, H. G. Schulze, C. G. Atkins, J. M. Piret, S. A. Aparicio, R. F. B. Turner, M. W. Blades, *Anal. Chem.* **2011**, 83, 6254.
- [39] L. E. Kamemoto, A. K. Misra, S. K. Sharma, M. T. Goodman, H. Luk, A. C. Dykes, T. Acosta, *Appl. Spectrosc.* **2010**, 64, 255.

SUPPORTING INFORMATION

Additional supporting information may be found online in the Supporting Information section at the end of this article.

How to cite this article: Y. Oka, M. Yoshida, A. Minoda, P. Leproux, M. M. Watanabe, H. Kano, *J Raman Spectrosc* **2021**, 52(12), 2572. <https://doi.org/10.1002/jrs.6142>